

1  
2  
3  
4  
5  
6  
7  
8  
9  
10  
11  
12  
13  
14  
15  
16  
17  
18  
19  
20  
21  
22

## The TSIS-1 Hybrid Solar Reference Spectrum

O. M. Coddington<sup>1</sup>, E. C. Richard<sup>1</sup>, D. Harber<sup>1</sup>, P. Pilewski<sup>1,2</sup>, T. N. Woods<sup>1</sup>, K. Chance<sup>3</sup>,  
X. Liu<sup>3</sup>, and K. Sun<sup>4,5</sup>

<sup>1</sup>Laboratory for Atmospheric and Space Physics, University of Colorado Boulder, USA.

<sup>2</sup>Department for Atmospheric and Oceanic Science, University of Colorado Boulder, USA.

<sup>3</sup>Harvard-Smithsonian Center for Astrophysics, Cambridge, USA.

<sup>4</sup>Department of Civil, Structural and Environmental Engineering, University at Buffalo, Buffalo, USA.

<sup>5</sup>Research and Education in eNergy, Environment and Water (RENEW) Institute, University at Buffalo, Buffalo, USA.

Corresponding author: Odele Coddington ([odele.coddington@lasp.colorado.edu](mailto:odele.coddington@lasp.colorado.edu))

†Additional author notes should be indicated with symbols (current addresses, for example).

### Key Points:

- The TSIS-1 Spectral Irradiance Monitor and Compact SIM instruments observe the Sun's irradiance spectrum at high accuracy.
- The TSIS-1 Hybrid Solar Reference Spectrum consists of high resolution solar line data normalized to the TSIS-1 SIM irradiance spectrum.
- The TSIS-1 Hybrid Solar Reference Spectrum has at least 0.01 nm spectral resolution, spans 202 to 2730 nm, and is accurate to 0.3 to 1.3%.

## 23 **Abstract**

24 We present a new solar irradiance reference spectrum representative of solar minimum  
25 conditions between solar cycles 24 and 25. The Total and Spectral Solar Irradiance Sensor-1  
26 (TSIS-1) Hybrid Solar Reference Spectrum (HSRS) is developed by applying a modified spectral  
27 ratio method to normalize very high spectral resolution solar line data to the absolute irradiance  
28 scale of the TSIS-1 Spectral Irradiance Monitor (SIM) and the CubeSat Compact SIM (CSIM).  
29 The high spectral resolution solar line data are the Air Force Geophysical Laboratory ultraviolet  
30 solar irradiance balloon observations, the ground-based Quality Assurance of Spectral  
31 Ultraviolet Measurements In Europe Fourier transform spectrometer solar irradiance  
32 observations, the Kitt Peak National Observatory solar transmittance atlas, and the semi-  
33 empirical Solar Pseudo-Transmittance Spectrum atlas. The TSIS-1 HSRS spans 202 nm to 2730  
34 nm at 0.01 to ~0.001 nm spectral resolution with uncertainties of 0.3% between 400 and 2365  
35 nm and 1.3% at wavelengths outside that range.

## 36 **Plain Language Summary**

37 The Sun's irradiance spectrum is used in many applications, such as constraining the solar  
38 forcing in climate models and converting measured satellite radiance to reflectance. A growing  
39 body of literature has provided evidence that the currently available solar reference spectra differ  
40 by more than their reported uncertainties. Such differences lead to biased results when different  
41 reference spectra are adopted in the aforementioned applications. This motivates our work to  
42 provide a new high-resolution solar reference spectrum at higher accuracy than any previously  
43 reported. Our ability to produce such a dataset is due to the state-of-the-art measurements of the  
44 Sun's irradiance spectrum made since March 2018 by the next-generation Spectral Irradiance  
45 Monitor (SIM) instrument on the Total and Spectral Solar Irradiance Sensor-1 (TSIS-1) satellite  
46 mission and the Compact SIM (CSIM) technology demonstration mission. The TSIS-1 SIM and  
47 CSIM have order-of-magnitude reduction in uncertainty relative to predecessor instruments  
48 primarily because of a first-of-its-kind spectral radiometric calibration facility capable of  
49 characterizing the instruments to higher fidelity. We develop this new, high-resolution, solar  
50 irradiance reference spectrum by adjusting high spectral resolution solar line data to the  
51 irradiance scale of the more accurate, but lower spectral resolution, TSIS-1 SIM and CSIM  
52 observations.

## 53 **1 Introduction**

54 Reference solar irradiance spectra have broad utility in atmospheric science and climate  
55 applications. For example, the incoming solar spectral irradiance is used to convert measured  
56 satellite radiance to reflectance (e.g., Wielicki et al., 2013) and as the upper boundary condition  
57 in radiative transfer models used, for example, in remote sensing algorithms and renewable  
58 energy research (e.g., Berk et al., 2014; Apell & McNeill, 2019). Some instruments use the  
59 absorption lines in a reference spectrum for wavelength calibration (e.g., Kang et al., 2020).  
60 Some instruments also use the Sun as a radiometric calibration source for stability monitoring,  
61 which first requires a solar reference spectrum as a baseline against which to quantify  
62 instrumental changes (e.g., Pan & Flynn, 2015). Instruments that assess the stability of their  
63 radiometric calibration relative to the moon (e.g., Werdell et al., 2019) indirectly rely on a solar  
64 reference spectrum to convert lunar radiance to reflectance using, for example, the RObotic  
65 Lunar Observatory (ROLO) model (Kieffer & Stone, 2005). Solar reference spectra are also

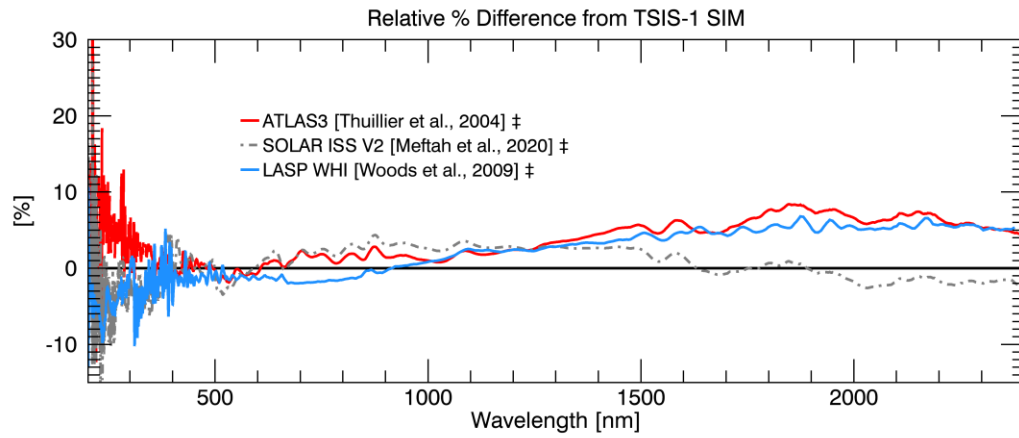
66 used to constrain solar irradiance variability models (e.g., Coddington et al. 2016) which climate  
67 models use to specify solar forcing of climate change (e.g., Kunze et al., 2020).

68 A number of existing solar reference spectra are available for the applications listed  
69 above. Some are from direct observations of the Sun's irradiance from one or more satellite  
70 instruments. These have relatively high reported accuracy and relatively low (0.1 nm or poorer)  
71 spectral resolution compared to ground-based observations and are typically specific to certain  
72 solar activity levels (e.g., Thuillier et al., 2004; Woods et al., 2009; Meftah et al., 2020). Other  
73 solar reference spectra are constructed by normalizing high spectral resolution solar lines to a  
74 high accuracy, low spectral resolution, irradiance spectrum (e.g., Chance and Kurucz, 2010).  
75 Still other reference spectra are created by concatenating independent datasets from different  
76 spectral regions (e.g., Gueymard, 2003). Such approaches are necessary because the technology  
77 does not exist to measure the Sun's spectrum over a broad spectral range from a single  
78 instrument with both high accuracy and high (0.01 nm or finer) spectral resolution. A growing  
79 body of literature has identified disagreements between the available solar reference spectra  
80 irradiance scales with independent measurements that often exceed the quoted accuracies,  
81 particularly at near-infrared wavelengths where differences reaching 8% have been reported  
82 (e.g., Elsey et al., 2017).

83 Since March 2018, NASA's Total and Spectral Solar Irradiance Sensor-1 (TSIS-1)  
84 Spectral Irradiance Monitor (SIM) hosted on the International Space Station has observed solar  
85 spectral irradiance with lower radiometric uncertainty ( $< 0.3\%$ ) over the majority of the spectrum  
86 than that attained by any previous instrument (Richard et al., 2020). Since 2019, independent  
87 observations of solar spectral irradiance measurements have also been made by the Compact  
88 SIM (CSIM) instrument from a CubeSat technology demonstration mission (Richard et al., 2019;  
89 Tomlin et al., 2020). CSIM observations span 200 nm to 2800 nm, thereby extending further into  
90 the infrared than the TSIS-1 SIM that spans 200 nm to 2400 nm. A mutual validation of the  
91 TSIS-1 SIM and CSIM irradiance scales was demonstrated by less than 1% disagreement in  
92 concurrent observations (Stephens et al., 2020).

93 Figure 1 shows the spectral difference of three established solar irradiance reference  
94 spectra to TSIS-1 SIM with disagreements reaching or exceeding 10%, particularly in the  
95 ultraviolet and near-infrared portions of the spectrum. The ATLAS-3 spectrum (Thuillier et al.,  
96 2004), perhaps the most widely-used solar reference in Earth science applications, is a composite  
97 of solar observations from November, 1994 by five different instruments on two different  
98 platforms: the Upper Atmospheric Research Satellite and the ATLAS shuttle mission.  
99 Additionally, high resolution modeled solar absorption features from Kurucz (1995) were  
100 inserted into the lower resolution observations from the visible through the near-infrared.  
101 Reported ATLAS-3 uncertainties are 2-3%. Another frequently used solar reference spectrum is  
102 the Laboratory for Atmospheric and Space Physics (LASP) Whole Heliospheric Interval (WHI)  
103 (Woods et al., 2009). The LASP WHI is a composite of solar observations with the majority of  
104 the spectrum measured during April, 2008 by two instruments on the Solar Radiation and  
105 Climate Experiment (SORCE) satellite, SOLSTICE and SIM. The observations from SORCE  
106 SIM, the predecessor to the TSIS-1 SIM, were adjusted upwards by as much as 8% for  
107 wavelengths above 1350 nm to agree with the ATLAS-3 spectrum in a recalibration that has  
108 been discussed with reference to a systematic bias (Harder et al., 2010). Therefore, the LASP  
109 WHI and ATLAS-3 reference spectra are not independent above 1350 nm. Reported LASP WHI  
110 uncertainties are 1-3% for wavelengths above 300 nm. Yet another solar reference spectrum is

111 SOLAR-ISS version 2 (Meftah et al., 2020). SOLAR-ISS is from a newer version of the SOLAR  
 112 SPECTrometer (SOLSPEC) than what was flown during the ATLAS era. The SOLAR-ISS  
 113 reference irradiance baseline spectrum is from April, 2008 for wavelengths spanning 165-656  
 114 nm and an average over a six year period at wavelengths above 656 nm. Revised engineering  
 115 corrections, improved calibrations, and advanced thermal and degradation corrections are  
 116 reported as the reason for the changes in the baseline between the earlier ATLAS-3 and the  
 117 newer SOLAR-ISS spectra. Similar to the ATLAS-3 approach, higher spectral resolution lines  
 118 have been incorporated into SOLAR-ISS. The mean reported SOLAR-ISS uncertainty from 165  
 119 to 3000 nm is 1.26%, with uncertainties as low as 0.4-0.6% between 800 to 1700 nm and  
 120 reaching, or exceeding, 2% below 400 nm and above 2200 nm. Hilbig et al. (2018) summarize  
 121 the characteristics of other solar reference spectra than those discussed here.



122

123 **Figure 1.** Percent relative difference between the ATLAS-3, SOLAR-ISS (v2) and LASP WHI  
 124 solar reference spectra from TSIS-1 SIM. All datasets have been convolved to the TSIS-1 SIM  
 125 spectral resolution prior to computing the difference as  $(\text{Reference} - \text{TSIS-1 SIM}) / \text{TSIS-1 SIM}$   
 126  $\times 100$ .

127 The results shown in Figure 1 motivate our work to produce a new solar reference  
 128 spectrum, the *TSIS-1 Hybrid Solar Reference Spectrum (TSIS-1 HSRS)*, by adjusting high  
 129 spectral resolution solar line data to the absolute, SI-traceable, irradiance scale of the more  
 130 accurate, but lower spectral resolution, TSIS-1 SIM and CSIM observations. The methodology to  
 131 develop the HSRS is described in Section 2 and the datasets are described in Section 3. In  
 132 Section 4, we present our results, describe our uncertainty assessment, and compare the HSRS to  
 133 independent datasets. Concluding statements follow in Section 5.

## 134 2 Methodology

135 We apply a modified version of the spectral ratio method to develop the HSRS. In this  
 136 method, a wavelength-dependent scaling factor adjusts high spectral resolution datasets ( $\beta$ ) to  
 137 match a lower resolution but higher accuracy spectrum ( $\alpha$ ). The scaling factor,  $Q$ , is derived  
 138 from the ratio of the  $\alpha$  and  $\beta$  datasets after first convolving both to the same spectral resolution  
 139 and interpolating to a common sampling grid. The  $\alpha$  and  $\beta$  datasets are described in Section 3.

140 Typically, the  $Q$  factor is derived after a single-step convolution (Eq. 1) of the  $\beta$  dataset  
 141 with the instrument line shape of the  $\alpha$  dataset ( $ILS_\alpha$ ) that degrades the resolution of the  $\beta$

142 dataset ( $\beta^*$ ) to match that of the  $\alpha$  dataset (e.g., Kang et al., 2017; Dobber et al., 2008). In our  
 143 modification, we apply a two-step convolution in deriving our  $Q$  factor: the first step is as  
 144 described by Eq. 1 and the second step degrades both  $\beta^*$  and  $\alpha$  datasets to a common spectral  
 145 resolution (denoted  $\beta^{**}$  and  $\alpha^{**}$ , respectively) that is coarser than that of the original  $\alpha$  dataset.  
 146 We accomplish this by convolution with a Gaussian filter ( $\mathbb{N}$ ) of specified standard deviation ( $\sigma$ )  
 147 (Eq. 2). The two-step convolution reduces the impacts of any uncertainty in  $ILS_\alpha$  on the  $Q$  factor  
 148 defined in Eq. 3, where the subscript  $\ddagger$  denotes an interpolation of the  $\beta^{**}$  dataset to the  $\alpha^{**}$   
 149 sampling grid. Finally, the adjusted  $\beta$  dataset (denoted by  $\mathbf{Y}$ ) is computed from the product of the  
 150 native  $\beta$  dataset and the  $Q$  factor, where the subscript  $\dagger$  denotes an interpolation of the  $Q$  factor  
 151 to the native  $\beta$  sampling grid (Eq. 4).

$$\beta^* = \beta \otimes ILS_\alpha \quad (1)$$

$$\beta^{**} = \beta^* \otimes \mathbb{N}(\sigma) \text{ and } \alpha^{**} = \alpha \otimes \mathbb{N}(\sigma) \quad (2)$$

$$Q = \alpha^{**} / \beta_{\ddagger}^{**} \quad (3)$$

$$\mathbf{Y} = \beta \times Q_{\dagger} \quad (4)$$

152  $\mathbf{Y}$  represents the  $\beta$  datasets at the absolute irradiance scale of the  $\alpha$  spectrum.  $\mathbf{Y}$  datasets  
 153 differ from the native  $\beta$  datasets in their broad baseline features, but share the same native  
 154 spectral and sampling resolutions. The TSIS-1 HSRS is the concatenation of these  $\mathbf{Y}$  datasets. In  
 155 transition regions, where one  $\mathbf{Y}$  dataset overlaps in wavelength with another, we adopt an  
 156 average of the irradiance values for the HSRS.

### 157 **3 Data**

#### 158 **3.1 High Accuracy ( $\alpha$ ) Spectrum**

159 Our high accuracy  $\alpha$  spectrum is from TSIS-1 Spectral Irradiance Monitor (SIM) and  
 160 Compact SIM (CSIM) space-based observations of solar spectral irradiance. TSIS-1 SIM has  
 161 measured daily spectral irradiance between 200-2400 nm since March 2018. The CSIM dataset,  
 162 spanning 210-2800 nm, began in late-March 2019. The SIM instruments are prism spectrometers  
 163 with variable spectral resolution of approximately 0.25 to 40 nm (Richard et al., 2019; 2020).  
 164 TSIS-1 SIM and CSIM data are available from these websites:  
 165 <https://lasp.colorado.edu/home/tsis/data/ssi-data/> and [https://lasp.colorado.edu/home/csim/data-](https://lasp.colorado.edu/home/csim/data-and-ham-radio/)  
 166 [and-ham-radio/](https://lasp.colorado.edu/home/csim/data-and-ham-radio/).

167 TSIS-1 SIM has order-of-magnitude reductions in radiometric uncertainty relative to the  
 168 heritage SORCE SIM instrument (Harder et al., 2005) through an extensive component level  
 169 calibration program that characterized the instrument as an absolute sensor and verified the  
 170 instrument in irradiance across the spectrum against an SI-traceable cryogenic radiometer using  
 171 stable tunable laser sources (Richard et al. 2020). The instrument level validation and final end-  
 172 to-end absolute calibration placed relative pre-launch accuracy uncertainties at 0.24% (>400 nm)  
 173 to 0.41% (<400 nm). On-orbit calibration stability is maintained by instrument degradation

174 corrections that utilize observations made by redundant and independent instrument channels  
175 that are exposed to the Sun at varying duty cycles (Mauceri et al., 2020).

176 CSIM is a 6U CubeSat technology demonstration mission for the NASA Earth Science  
177 Technology Office In-Space Validation of Earth Science Technologies program. CSIM  
178 radiometric accuracy is tied to the same SI-traceable cryogenic radiometer with the same laser  
179 sources used in the TSIS-1 SIM calibrations, but by calibration transfer as opposed to absolute  
180 calibration verification. Based on this calibration, the CSIM measurement uncertainty is <1%  
181 from 300-2000 nm, increasing to 1.26% above 2000 nm (Richard et al., 2019).

182 Specifically, the  $\alpha$  spectrum in our study, from 200 to 2365 nm, is an average of daily  
183 TSIS-1 SIM irradiance observations from 1-7 December 2019, which is a time period that  
184 coincides with the solar activity minimum between solar cycles 24 and 25 based on a 13-month  
185 smoothing of the sunspot number (<https://www.swpc.noaa.gov/news/solar-prediction-scientists-announce-solar-cycle-25>). We extend this averaged spectrum from 2365 to 2730 nm with  
186 averaged CSIM observations from April to September, 2019. The CSIM uncertainty includes the  
187 error contribution from neglecting solar variability at these infrared wavelengths. A wavelength-  
188 independent offset factor of 0.9921 ensures the CSIM irradiance portion of the  $\alpha$  spectrum (i.e.  
189  $\geq 2365$  nm) matches TSIS-1 SIM irradiance at 2365 nm. This 0.8% offset is within the 1.26%  
190 CSIM measurement uncertainty.  
191

### 192 3.2 High Spectral Resolution ( $\beta$ ) Datasets

193 The  $\beta$  datasets are the Air Force Geophysical Laboratory (AFGL) ultraviolet solar  
194 irradiance balloon observations, the ground-based Kitt Peak National Observatory (KPNO) solar  
195 transmittance atlas, the ground-based Quality Assurance of Spectral Ultraviolet Measurements In  
196 Europe (QASUME) Fourier transform spectrometer (QASUMEFTS) solar irradiance  
197 observations, and the semi-empirical Solar Pseudo-Transmittance Spectrum (SPTS) atlas. Brief  
198 descriptions of each are given below and key details can be found in the respective references.

199 Grating spectrometer observations of the Sun's ultraviolet irradiance from high-altitude  
200 balloons dating to the 1970's and 1980's by the Air Force Geophysical Laboratory (AFGL) (Hall  
201 & Anderson, 1991) are the only solar spectral irradiance dataset available to date between 200  
202 nm and 310 nm with a spectral resolution of 0.01 nm or better. Corrections for atmospheric  
203 ozone absorption attenuation were applied to the data. The spectral and sampling resolution of  
204 the AFGL irradiance dataset are 0.01 nm and the radiometric uncertainty is typically 5-10%, but  
205 can reach 25% near 200 nm.

206 Additional high resolution data are solar transmittances between 300 and 1000 nm  
207 (Kurucz, 2005) derived from at the Kitt Peak National Observatory (KPNO) ground-based  
208 Fourier transform spectroradiometer (FTS) observations between 296 and 1300 nm at  $\sim 0.001$  nm  
209 resolution (Kurucz et al., 1984). The conversion from FTS observations to a transmittance was  
210 achieved by an iterative, multi-step process (Kurucz, 2005). The steps involved removing  
211 continuum atmospheric absorption features based on a model followed by the estimation and  
212 removal of the solar continuum with subjective fits of the FTS observations to a simulated solar  
213 spectrum. Sharp telluric spectral features, attributed to molecules in Earth's atmosphere, were  
214 identified with the HITRAN database (Rothman et al., 2005) and removed. The KPNO residual

215 irradiance wavelength scale accuracy, reassessed for this study, is found to be better than  $3.2 \times 10^{-4}$   
216 nm above 305 nm and better than  $3.0 \times 10^{-3}$  nm at shorter wavelengths, unchanged from that  
217 reported in Chance and Kurucz (2010).

218 An additional source is the high-resolution extraterrestrial solar irradiance spectrum  
219 measured by an FTS between 305 nm and 380 nm from a high-altitude, ground location during  
220 the Quality Assurance of Ultraviolet Measurements In Europe (QASUMEFTS) campaign. The  
221 measured spectrum was extended down to 300 nm and up to 500 nm with the KPNO atlas  
222 (Gröbner et al., 2017). The extraterrestrial solar spectrum was derived from QASUME  
223 observations by the Langley plot technique (e.g., Arvesen et al., 1969). The FTS observations  
224 were adjusted to the absolute irradiance scale of a lower-resolution, reference spectroradiometer  
225 with accuracy traceable to the primary spectral irradiance standard of the Physikalisch  
226 Technische Bundesanstalt (PTB) laboratory in Germany. QASUMEFTS radiometric uncertainty  
227 reaches 4% at wavelengths lower than 310 nm and 2% between 310 and 500 nm. The spectral  
228 resolution of QASUMEFTS is better than 0.025 nm and uncertainty in the wavelength-scale is  
229 0.01 nm or better.

230 Version 2016 of the ‘disk-integrated’ Solar Pseudo-Transmittance Spectrum (SPTS)  
231 (Toon, 2014) contains the transmittance from 40,000 solar absorption lines spanning 600-26316  
232  $\text{cm}^{-1}$  (380-16600 nm), sampled every 0.01  $\text{cm}^{-1}$ . It is an empirically-generated dataset, where  
233 telluric line contributions to the observed spectra from multiple FTS instruments (both ground-  
234 and space-based) are identified with the HITRAN database and iteratively removed. Measured  
235 KPNO spectra are the predominant observation source in the SPTS database, supplemented with  
236 observations from high-altitude balloons and satellites (Toon, 2013).

237 We adopt a vacuum wavelength scale for the HSRS. Conversions from air-to-vacuum  
238 wavelengths were applied to the AFGL and QASUMEFTS datasets using Edlén’s (1966)  
239 standard air dispersion formula.

## 240 **4 Results**

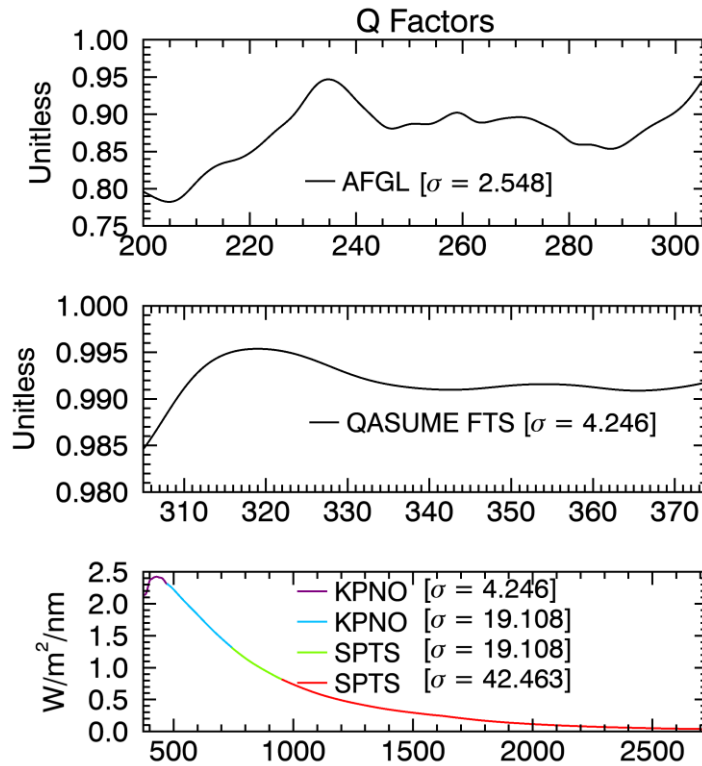
241 In this section, we present the TSIS-1 Hybrid Solar Reference Spectrum (HSRS) and  
242 make comparisons to independent datasets.

### 243 4.1 $Q$ factor

244 When the spectral ratio method is used to adjust an *irradiance* dataset, the  $Q$  factor is  
245 unitless and represents a magnitude adjustment to the radiometric calibration of the original  
246 dataset. However, when the method is applied to adjust a *solar transmittance* dataset, the  $Q$   
247 factor has units of solar spectral irradiance ( $\text{Watts/m}^2/\text{nm}$ ) and approximates the continuum of  
248 the Sun’s spectral irradiance when devoid of absorption and emission features. In either case, the  
249  $Q$  factor adjusts broad, continuum features while leaving fine spectral features undisturbed.

250 Figure 2 shows the  $Q$  factors used to produce the HSRS at the high accuracy  $\alpha$  irradiance  
251 scale. The adjustments are smaller than 25% for AFGL and 2.5% for QASUMEFTS datasets,  
252 which falls within their respective reported radiometric uncertainties. The adjustments for the

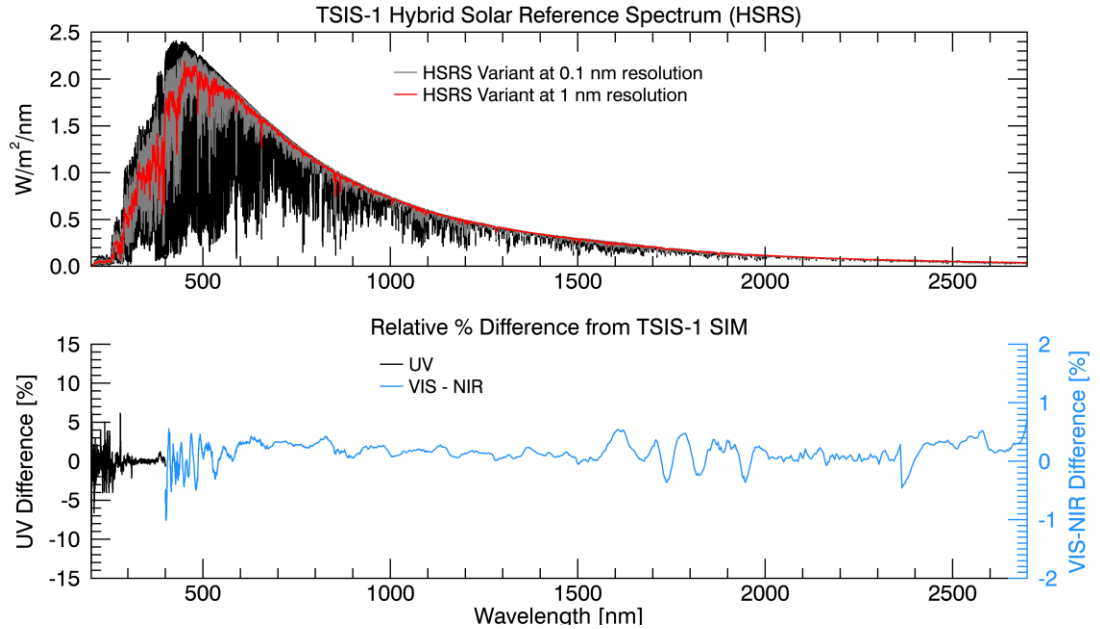
253 KPNO and SPTS solar transmittance datasets have the expected spectral shape of the Sun's  
 254 continuum.



255

256 **Figure 2.** The wavelength-dependent  $Q$  factors used to adjust the AFGL, QASUMEFTS, KPNO  
 257 and SPTS datasets to the absolute radiometric scale of the TSIS-1 SIM and CSIM instruments  
 258 using the Gaussian convolution filters (see Eq. 2) of the specified standard deviation ( $\sigma$ ) reported  
 259 in the legends.

260 Applying the  $Q$  factors to the high resolution  $\beta$  datasets forms the TSIS-1 HSRS shown  
 261 in Figure 3 (top; black) at 0.01 to  $\sim 0.001$  nm spectral resolution and spanning 202 to 2730 nm.  
 262 We also produce four variants of the HSRS by applying Gaussian convolution kernels in order to  
 263 standardize the reference spectrum to fixed, lower spectral resolutions; two of these variants are  
 264 also shown in Figure 3. The integrated solar spectral irradiance of the HSRS and the HSRS  
 265 variants matches the integral of the  $\alpha$  spectrum between 202 and 2730 nm ( $1324.94 W m^{-2}$ ) to  
 266 within 0.2%. We produce an additional variant of the HSRS dataset (not shown) over the spectral  
 267 range 202 to 500 nm with variable Gaussian convolution kernels that approximate the spectral  
 268 resolution, but not the true spectral shape, of the SOLAR Solar-Stellar Irradiance Comparison  
 269 Experiment (SOLSTICE) (McClintock et al., 2005) and the Aura Ozone Monitoring Instrument  
 270 (OMI) (Levelt et al., 2006). This final variant has utility for developing new, higher resolution,  
 271 solar irradiance variability models (Lean et al., 2020). The HSRS and its variants, summarized in  
 272 Table 1, are reported on fixed wavelength grids of at least 4 points per resolution element.



273

274 **Figure 3.** (top) The TSIS-1 Hybrid Solar Reference Spectrum (black) and two HSRS variants at  
 275 lower resolution. (bottom) The relative percent difference of the HSRS from the high accuracy  
 276 ( $\alpha$ ) spectrum, computed identically as in Figure 1, with separate percent difference y-axis scales  
 277 for the ultraviolet (UV; < 400 nm) and visible-to-near-infrared (VIS-NIR; >400 nm) portions of  
 278 the spectrum.

279 Figure 3 (bottom) shows the relative percent difference between the HSRS and the high  
 280 accuracy  $\alpha$  spectrum. The HSRS has been convolved with the measured TSIS-1 SIM and CSIM  
 281 instrument line shapes prior to taking the difference. Near-identical results (not shown) are  
 282 obtained when computing the relative difference for the HSRS variants.

283 **Table 1.** A summary of the specifications for the TSIS-1 Hybrid Solar Reference Spectrum  
 284 (HSRS) dataset and its variants. Identified for each HSRS spectrum is the spectral range covered  
 285 by the high resolution  $\beta$  datasets, the spectral and sampling resolutions, and the uncertainty. For  
 286 the purposes of this study, spectral resolution of the HSRS variants is defined by the full-width  
 287 half-maximum value of the Gaussian convolution kernel.

288

File Name	High resolution Datasets and Wavelength Coverage (nm)	Spectral Resolution	Sampling resolution	Uncertainty (%)
TSIS-1 HSRS	AFGL: 202 - 306.5 QASUMEFTS: 305.5 - 373.6 KPNO: 373.5 - 745 SPTS: 743 - 2730	Varies; equal to that of the original high resolution, $\beta$ , datasets	0.001 nm	<400 nm = 1.3 400-2365 nm = 0.3 >2365 nm = 1.3
TSIS-1 HSRS 'p005nm'	Same as TSIS-1 HSRS	0.025 nm (below 374 nm) 0.005 nm (above 374 nm)	0.001 nm	Same as above
TSIS-1 HSRS 'p025nm'	Same as TSIS-1 HSRS	0.025 nm	0.005 nm	Same as above

TSIS-1 HSRS 'p1nm'	Same as TSIS-1 HSRS	0.1 nm	0.025 nm	Same as above
TSIS-1 HSRS '1nm'	Same as TSIS-1 HSRS	1 nm	0.2 nm	Same as above
TSIS-1 HSRS 'SOL-OMI'	AFGL: 202 - 309.8 QASUMEFTS: 306.4 - 373.5 KPNO: 373.3 - 500	0.048 nm (below 310 nm) 0.42 nm (310 to 360 nm) 0.62-0.64 nm (360 to 500 nm)	0.025 nm	<400 nm = 1.3 400-500 nm = 0.3

289

290

#### 4.2 Uncertainties

291

292

293

294

295

296

297

298

299

The total TSIS-1 HSRS uncertainty (Table 1; far right) is the root-sum-square of the following error sources: the uncertainties of the TSIS-1 SIM and CSIM measurements that comprise the  $\alpha$  spectrum and the methodology accuracy. We estimate this second component from the  $1-\sigma$  standard deviation of the relative percent difference of the HSRS and the  $\alpha$  spectrum (Figure 3; bottom). The HSRS uncertainty is equivalent to 0.3% over most of the spectrum, increasing to 1.3% below 400 nm and above 2365 nm. It reflects the uncertainty of the HSRS *for the same spectral resolution as the TSIS-1 and the CSIM instruments*. At very high spectral resolution, the relative differences in individual lines from different solar line databases can reach several tens of percent (not shown).

300

#### 4.3 Comparison to Other Datasets

301

302

303

304

305

306

307

The combined results of Figures 1 and 3 establish that the HSRS differs from the ATLAS-3 and LASP WHI solar reference spectra on the order of several percent between 500 nm and 1300 nm, increasing to 8-10% for wavelengths outside of that range. The HSRS differs from the SOLAR-ISS reference spectrum by +3.3% ( $\sim +0.06 \text{ W m}^{-2}$ ) near the peak of the solar spectrum at 520 nm and by -2 to -4% ( $-0.01$  to  $-0.03 \text{ W m}^{-2}$ ) between 800 nm and 1400 nm. In the ultraviolet, differences between the HSRS and SOLAR-ISS can approach 10%. Above 1500 nm, however, the agreement is generally within 2%.

308

309

310

311

312

313

314

315

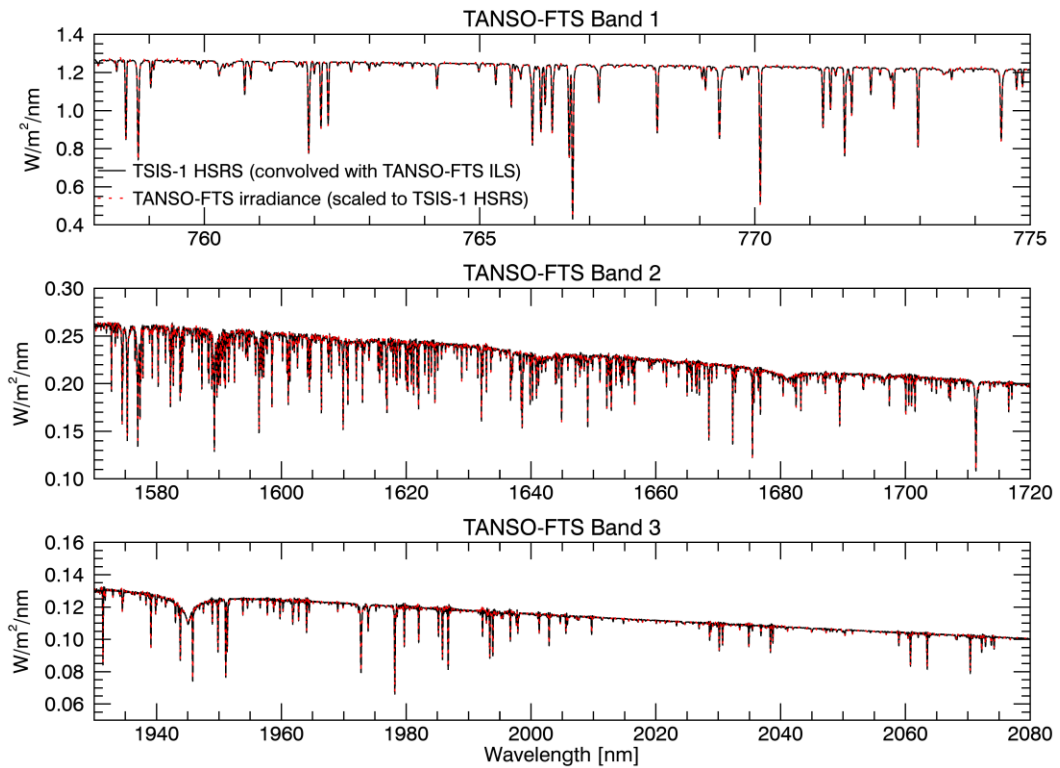
316

317

318

319

In Figure 4, we show a comparison of the HSRS to high-resolution TANSO Fourier Transform Spectrometer (TANSO-FTS) observations obtained during solar calibration scans of the Greenhouse Gases Observing Satellite (GOSAT) mission (Kuze et al., 2009). For the comparison, the HSRS resolution has been reduced to match that of the TANSO-FTS instrument. We also apply adjustments to the TANSO-FTS data. First, we correct the wavelength scale for the Doppler shift that occurs with changing spacecraft velocity. Second, we convert the s- and p-polarized solar radiance to solar irradiance under the assumption of a perfect solar diffuser plate. Third, we average the Doppler-corrected, s- and p-polarized irradiance to get the unpolarized solar irradiance spectrum. Finally, we adjust the irradiance scale to match that of the HSRS using the spectral ratio method described in Section 2. The resulting  $1-\sigma$  standard deviation of the HSRS and TANSO-FTS relative percent difference is smaller than 0.4% in all bands (not shown), demonstrating robust HSRS solar line positions and depths in these wavelength ranges.



320

321 **Figure 4.** A comparison of the TSIS-1 HSRS to a GOSAT TANSO-FTS solar irradiance  
 322 spectrum derived from solar radiances measured in three bands during calibration scans (see  
 323 text).

## 324 5 Conclusions

325 The TSIS-1 Hybrid Solar Reference Spectrum (HSRS) is a new solar irradiance reference  
 326 spectrum developed by normalizing high spectral resolution solar line data to the absolute  
 327 irradiance scale of the TSIS-1 SIM and CSIM observations at solar minimum between solar  
 328 cycles 24 and 25. TSIS-1 SIM and CSIM observe the Sun's irradiance spectrum at higher  
 329 accuracy than attained by predecessor instruments and, notably, show the near-infrared solar  
 330 spectrum is reduced in magnitude by up to 8-10% relative to some other often-used solar  
 331 reference spectra. Therefore, the HSRs provides an important new constraint for science  
 332 analyses in a broad array of fields.

333 The HSRs spans 202 to 2730 nm, encompassing an integrated energy that exceeds 97% of the  
 334 total solar irradiance. The HSRs accuracy is 0.3% to 1.3% and the spectral resolution is 0.01 nm  
 335 to  $\sim 0.001$  nm. Variants of the HSRs are also provided for lower, fixed spectral resolutions.

## 336 Acknowledgments, Samples, and Data

337 The TSIS-1 HSRs is available from <https://lasp.colorado.edu/lisird/>. The authors extend  
 338 their gratitude to the teams responsible for the development and maintenance of the AFGL,  
 339 QASUMEFTS, KPNO, and JPL SPTS databases. Additionally, the authors extend their gratitude  
 340 to F. Kataoka and A. Kuze for provision and assistance with the GOSAT solar calibration  
 341 radiance data, to M. Snow for provision of the SORCE SOLSTICE instrument line shape

342 information, and to S. Marchenko for the Aura OMI instrument line shape information. OC, ER,  
343 DH, PP, and TW are grateful for the support of the NASA TSIS-1 project (80GSFC18C0056)  
344 and NASA's Solar Irradiance Science Team (80NSSC18K1304) in performing this analysis.  
345 Authors at the Harvard-Smithsonian Center for Astrophysics thank NASA for ongoing support  
346 for development of satellite measurements of the Earth's atmosphere.

## 347 **References**

- 348 Apell, J. N., & McNeill, K. (2019), Updated and validated solar irradiance reference spectra for  
349 estimating environmental photodegradation rates. *Environ. Sci.: Processes Impacts*, 21, 2153-  
350 2153.
- 351 Arvesen, J. C., Griffin, R. N., & Pearson, B. D. (1969), Determination of Extraterrestrial Solar  
352 Spectral Irradiance from a Research Aircraft. *Appl. Opt.* 8, 2215-2232.
- 353 Berk, A., Conforti, P., Kennett, R., Perkins, T., Hawes, F., & van den Bosch, J.,  
354 (2014), MODTRAN6: a major upgrade of the MODTRAN radiative transfer code. *Proc. SPIE*  
355 *9088, Algorithms and Technologies for Multispectral, Hyperspectral, and Ultraspectral Imagery*  
356 *XX*, 90880H. doi:10.1117/12.2050433
- 357 Chance, K., & Kurucz, R. L. (2010), An improved high-resolution solar reference spectrum for  
358 earth's atmosphere measurements in the ultraviolet, visible, and near infrared. *J. of Quant. Spec.*  
359 *and Rad. Tran.*, 111(9), 1289-1295.
- 360 Coddington, O., Lean, J. L., Pilewskie, P., Snow, M., & Lindholm, D. (2016), A Solar Irradiance  
361 Climate Data Record. *Bull. Amer. Meteor. Soc.*, 97, 1265–1282. [https://doi.org/10.1175/BAMS-](https://doi.org/10.1175/BAMS-D-14-00265.1)  
362 [D-14-00265.1](https://doi.org/10.1175/BAMS-D-14-00265.1)
- 363 Dobber, M., Voors, R., Dirksen, R., Kleipool, Q., & Levelt, P. (2008), The High-Resolution  
364 Solar Reference Spectrum between 250 and 550 nm and its Application to Measurements with  
365 the Ozone Monitoring Instrument. *Sol. Phys.*, 249, 281–291. [https://doi.org/10.1007/s11207-008-](https://doi.org/10.1007/s11207-008-9187-7)  
366 [9187-7](https://doi.org/10.1007/s11207-008-9187-7)
- 367 Edlén, B. (1966), The Refractive Index of Air, *Metrologia*, 2(2).
- 368 Elsey, J., Coleman, M.D., Gardiner, T., & Shine, K.P. (2017), Can measurements of the near-  
369 infrared solar spectral irradiance be reconciled? A new ground-based assessment between 4,000  
370 and 10,000 cm<sup>-1</sup>–110,000 cm<sup>-1</sup>. *Geophys. Res. Lett.* 44(19), 10071.
- 371 Gröbner, J., Kröger, I., Egli, L., Hülsen, G., Riechelmann, S., & Sperfeld, P. (2017), The high-  
372 resolution extraterrestrial solar spectrum (QASUMEFTS) determined from ground-based solar  
373 irradiance measurements. *Atmos. Meas. Tech.*, 10, 3375–3383. [https://doi.org/10.5194/amt-10-](https://doi.org/10.5194/amt-10-3375-2017)  
374 [3375-2017](https://doi.org/10.5194/amt-10-3375-2017)
- 375 Gueymard, C. A. (2003), The sun's total and spectral irradiance for solar energy applications and  
376 solar radiation models. *Sol. Energy*, 76, 423–453.
- 377 Hall, L. A., & Anderson, G. P. (1991), High resolution solar spectrum between 200 and 3100 Å.  
378 *J. Geophys. Res.*, 12927-12931. <https://doi.org/10.1029/91JD01111>
- 379 Harder J., Lawrence G., Fontenla J., Rottman G., & Woods T. (2005), *The Spectral Irradiance*  
380 *Monitor: Scientific Requirements, Instrument Design, and Operation Modes*. In: Rottman G.,

- 381 Woods T., George V. (eds) The Solar Radiation and Climate Experiment (SORCE). Springer,  
 382 New York, NY. [https://doi.org/10.1007/0-387-37625-9\\_9](https://doi.org/10.1007/0-387-37625-9_9)
- 383 Harder, J.W., Thuillier, G., Richard, E.C., Brown, S. W., Lykke, K. R., Snow, M., et al. (2010),  
 384 The SORCE SIM Solar Spectrum: Comparison with Recent Observations. *Sol. Phys.*, 263, 3–24.  
 385 <https://doi.org/10.1007/s11207-010-9555-y>
- 386 Hilbig, T., Weber, M., Bramstedt, K., Noël, S., Burrows, J. P., Krijger, J. M., et al. (2018), The  
 387 New SCIAMACHY Reference Solar Spectral Irradiance and Its Validation. *Sol. Phys.*, 293, 121.  
 388 <https://doi.org/10.1007/s11207-018-1339-9>
- 389 Kang, M. Ahn, M-H., Liu, X., Chance, K., Sun, K., & Kim, J. (2017), High Resolution  
 390 Reference Solar Spectrum for TEMPO/GEMS and beyond. *GSICS annual meeting, 2017 Annual*  
 391 *GSICS Joint Working Groups Meeting*, 20 – 24 March 2017, Madison, USA Available online  
 392 from  
 393 [http://gsics.atmos.umd.edu/pub/Development/20170320/4g\\_Mina\\_High\\_resolution\\_reference\\_solar\\_spectrum\\_for\\_%20GEMS\\_and%20\\_TEMPO.pdf](http://gsics.atmos.umd.edu/pub/Development/20170320/4g_Mina_High_resolution_reference_solar_spectrum_for_%20GEMS_and%20_TEMPO.pdf) [Last accessed July 28, 2020].  
 394
- 395 Kang, M., Ahn, M.-H., Liu, X., Jeong, U., & Kim, J. (2020), Spectral Calibration Algorithm for  
 396 the Geostationary Environment Monitoring Spectrometer (GEMS). *Remote Sens.*, 12, 2846.
- 397 Kieffer, H. H., & Stone, T. C. (2005), The spectral irradiance of the moon. *Astron. J.*, 129, 2887-  
 398 2901.
- 399 Kunze, M., Kruschke, T., Langematz, U., Sinnhuber, M., Reddmann, T., & Matthes, K.  
 400 (2020), Quantifying uncertainties of climate signals in chemistry climate models related to the  
 401 11-year solar cycle – Part 1: Annual mean response in heating rates, temperature, and ozone.  
 402 *Atmos. Chem. and Physics*, 20(11). 6991-7019. [10.5194/acp-20-6991-2020](https://doi.org/10.5194/acp-20-6991-2020).
- 403 Kurucz, R. (2005), High Resolution Irradiance Spectrum from 300 to 1000 nm. *AFRL*  
 404 *Transmission Meeting*, 15-16 June 2005, Lexington, Mass. Available online from  
 405 <https://arxiv.org/pdf/astro-ph/0605029.pdf> [last accessed July 25, 2020].
- 406 Kurucz, R.L., & Bell, B. (1995), *Atomic Line List*, Smithsonian Astrophys. Obs., Cambridge,  
 407 Mass.
- 408 Kurucz, R.L., Furenlid, I., Brault, J., & Testerman. L. (1984), *Solar Flux Atlas from 296 to*  
 409 *1300nm*. National Solar Observatory, Sunspot, New Mexico, 240 pp.
- 410 Kuze, A., Suto, H., Nakajima, M., & Hamazaki, T. (2009), Thermal and near infrared sensor for  
 411 carbon observation Fourier-transform spectrometer on the Greenhouse Gases Observing Satellite  
 412 for greenhouse gases monitoring. *Appl. Opt.*, 48, 6716-6733.
- 413 Lean, J. L., Coddington, O., Marchenko, S. V., Machol, J., DeLand, M. T., & Kopp, G. (2020),  
 414 Solar irradiance variability: Modeling the measurements. *Earth and Space Science*, 7,  
 415 e2019EA000645. <https://doi.org/10.1029/2019EA000645>
- 416 Levelt, P. F., van den Oord, G. H. J., Dobber, M. R., Malkki, A., Visser, H., de Vries, J., et al.  
 417 (2006), The ozone monitoring instrument. *IEEE Transactions on Geoscience and Remote*  
 418 *Sensing*, 44(5), 1093-1101. Doi:10.1109/TGRS.2006.872333.
- 419 Mauceri, S., Richard, E., Pilewskie, P., Harber, D., Coddington, O., Béland, S., et al. (2020),  
 420 Degradation Correction of TSIS SIM, *Solar Physics*, accepted.

- 421 McClintock, W.E., Rottman, G.J. & Woods, T.N. (2005), Solar–Stellar Irradiance Comparison  
 422 Experiment II (Solstice II): Instrument Concept and Design. *Sol. Phys.*, 230, 225–258.  
 423 <https://doi.org/10.1007/s11207-005-7432-x>
- 424 Meftah, M., Damé, L., Bolsée, D., Pereira, N., Snow, M., Weber, M., et al. (2020), A New  
 425 Version of the SOLAR-ISS Spectrum Covering the 165 – 3000 nm Spectral Region. *Sol.*  
 426 *Phys.*, 295(14). <https://doi.org/10.1007/s11207-019-1571-y>
- 427 Pan, C., & Flynn, L. E. (2015), Solar observation of Ozone Mapping and Profiler Suite nadir  
 428 system during the first 3 years of on-orbit operation. *J. of Applied Remote*  
 429 *Sensing*, 9(1). <https://doi.org/10.1117/1.JRS.9.094095>
- 430 Richard, E., Harber, D., Drake, G., Rutkowski, J., Castleman, Z., Smith, M., et al. (2019),  
 431 Compact spectral irradiance monitor flight demonstration mission. *Proc. SPIE 11131, CubeSats*  
 432 *and SmallSats for Remote Sensing III*, 1113105. doi:10.1117/12.2531268.
- 433 Richard, E., Harber, D., Coddington, O., Drake, G., Rutkowski, J., Triplett, M., et al. (2020), SI-  
 434 traceable Spectral Irradiance Radiometric Characterization and Absolute Calibration of the TSIS-  
 435 1 Spectral Irradiance Monitor (SIM). *Remote Sens.*, 12(11), 1818.  
 436 <https://doi.org/10.3390/rs12111818>
- 437 Rothman, L. S., Jacquemart, D., Barbe, A., Chris Benner, D., Birk, M, Brown, L. R., et al.  
 438 (2005), The HITRAN 2004 molecular spectroscopic database. *JQSRT*, 96, 139-204
- 439 Stephens, G., Freeman, A., Richard, E., Pilewskie, P., Larkin, P., Chew, C., et al. (2020), The  
 440 Emerging Technological Revolution in Earth Observations. *Bull. Amer. Met. Soc.*, 101(3), E274-  
 441 E285. doi:10.1175/BAMS-D-19-0146.1
- 442 Thuillier, G., Floyd, L., Woods, T.N., Cebula, R., Hilsenrath, E., Hersé, M., & Labs, D. (2004),  
 443 Solar irradiance reference spectra. In: Pap, J.M., Fox, P., Fröhlich, C., Hudson, H.S., Kuhn, J.,  
 444 McCormack, J., North, G., Sprigg, W., Wu, S.T. (eds.) *Geophys. Monogr.* 141, 171.
- 445 Tomlin, N. A., Yung, C. S., Castleman, Z., Denoual, A. M., Drake, G., Farber, N., et al. (2020),  
 446 Overview of microfabricated bolometers with vertically aligned carbon nanotube absorbers. *AIP*  
 447 *Advances* 10, 055010. doi: 10.1063/5.0004025
- 448 Toon, G. C. (2014), *Solar line list for GGG2014*. TCCON data archive, hosted by the Carbon  
 449 Dioxide Information Analysis Center, Oak Ridge National Laboratory, Oak Ridge, Tennessee,  
 450 U.S.A., doi:10.14291/tcon.ggg2014.solar.R0/1221658, 2014. Available online from  
 451 [https://mark4sun.jpl.nasa.gov/toon/solar/solar\\_spectrum.html](https://mark4sun.jpl.nasa.gov/toon/solar/solar_spectrum.html) [last accessed July 25, 2020].
- 452 Toon, G. C. (2013), The Solar Spectrum: an Atmospheric Remote Sensing Perspective. Noble  
 453 Seminar, University of Toronto, 21 Oct. 2013, Toronto, Canada. Available online from  
 454 [https://mark4sun.jpl.nasa.gov/report/UT\\_seminar\\_Solar\\_Spectrum\\_Toon.pdf](https://mark4sun.jpl.nasa.gov/report/UT_seminar_Solar_Spectrum_Toon.pdf)
- 455 Werdell, P.J., Behrenfeld, M.J., Bontempi, P.S., Boss, E., Cairns, B., Davis, G.T., et al. (2019),  
 456 The Plankton, Aerosol, Cloud, ocean Ecosystem (PACE) mission: Status, science,  
 457 advances. *Bull. Amer. Meteor. Soc.*, 100(9), 1775-1794. doi:10.1175/BAMS-D-18-0056.1
- 458 Wielicki, B. A., Young, D. A., Mylnczak, M. G., Leroy, S., Corliss, J. Anderson, J. G., et al.  
 459 (2013), Achieving Climate Change Absolute Accuracy in Orbit. *Bull. Amer. Meteor. Soc.*, 94,  
 460 1519–1539. <https://doi.org/10.1175/BAMS-D-12-00149.1>.

461 Woods, T.N., Chamberlin, P.C., Harder, J.W., Hock, R.A., Snow, M., Eparvier, F.G., et al.  
462 (2009), Solar Irradiance Reference Spectra (SIRS) for the 2008 Whole Heliosphere Interval  
463 (WHI). *Geophys. Res. Lett.* 36(1), L01101.

464

465

466

467

468

469

470

471

472

473

474

475